Optical emission of graphene and electron-hole pair production induced by a strong terahertz field

I. V. Oladyshkin,[*] S. B. Bodrov, Yu. A. Sergeev, A. I. Korytin, M. D. Tokman, and A. N. Stepanov

Institute of Applied Physics, Russian Academy of Sciences, 46 Ul'yanov Street, 603950, Nizhny Novgorod, Russia

We report on experimental observation of optical emission of graphene induced by an intense terahertz (THz) pulse. P-doped chemical-vapor-deposition graphene with an initial Fermi energy of about 200 meV was used; optical photons were detected in the 2.0–3.5 eV range. Emission started when the THz field amplitude exceeded 100 kV/cm. For the THz fields from 200 to 300 kV/cm, the temperature of optical radiation was constant, while the number of emitted photons increased by several dozen times. This fact clearly indicates multiplication of electron-hole pairs induced by an external field and not electron heating. The experimental data are in good agreement with the theory of Landau-Zener interband transitions. It is shown theoretically that Landau-Zener transitions are possible even in the case of heavily doped graphene because the strong THz field removes quasiparticles from the region of interband transitions for several femtoseconds, which cancels the Pauli blocking effect.

I. INTRODUCTION

The nonlinear optical properties of graphene are currently being actively investigated in view of their prospective use in plasmonics, optoelectronics, and photonics [1]. The specific features of gapless dispersion of Dirac fermions, including the so-called Dirac cones, make graphene a unique material. In the neighborhood of the Dirac point, fermions have a massless dispersion law up to energies of the order of 1.5 eV and the high Fermi velocity $\upsilon_F \approx 10^8$ cm/s, thus providing ultrahigh nonlinear susceptibility (both quadratic and cubic) of graphene in the infrared and terahertz (THz) wave ranges [2–10]. The interaction of graphene with terahertz radiation is presently arousing particular interest from the viewpoint of various applications [11,12]. Monocycle terahertz pulses are also used for studying relaxation processes in graphene [13,14].

An interesting effect of the THz-pulse-initiated carrier multiplication (CM) was studied experimentally in [13]. This effect was attributed in [13] to impact ionization (II), i.e., to interband reverse Auger recombination. At the same time, according to the theoretical results obtained in [15] within the framework of the two-dimensional (2D) Fermi-liquid model, the Auger processes have low efficiency in the region of the linear dispersion law;[1] consequently, in the simulation made in [13] the Auger resonances were broadened "artificially" within the framework of the numerical scheme.[2] The CM effect was also observed in the case of optical pumping [14,16–22], when the contribution of the impact ionization to the formation of the electron population in the conducting band did not exceed 5%–10% [17].

It is worth noting that the ballistic (directly initiated by the field) interband transitions were neglected in [13] in view of the small photon energy, as compared to the typical kinetic energy of fermions in doped graphene. This approach, however, is justified only within the applicability of the perturbation method, when the energy of the quasiparticle interaction with an high frequency field is small compared to the energy of the resonance transition: $e\upsilon_F A/c \ll \hbar\omega$ (here, A is the vector potential amplitude). The typical field intensity $E \approx 100$ kV/cm for a frequency of 2 THz reported in [13] by no means corresponds to the given parameter region $e\upsilon_F A/c\hbar\omega \approx 30$. Note that nonlinear interaction of a strong THz field with graphene was studied experimentally in [23,24]; it was demonstrated that scattering processes do not have a significant influence on the formation of both interband and intraband currents.[3]

In our work, the ballistic CM mechanism under the action of intense THz pulses is studied experimentally and theoretically. We address the mechanism of Schwinger electron-hole pair production considered earlier in connection with transport processes in graphene [27–29]. This effect may also be adequately described within the framework of the Landau-Zener theory [30–32]. In dc fields, this effect usually makes a relatively small contribution to the current-voltage characteristic of a graphene sample that is observed at only weak doping [30,31]. We have derived a conclusion that, in the field of intense THz pulses, the ballistic mechanism of electron-hole pair generation, in contrast, plays a principal role in the formation of fermion distribution, even in the case of strong initial doping in chemical-vapor deposition (CVD) graphene, when the initial Fermi energy is of the order of hundreds of meV.

The structure of the paper is as follows. Section II is devoted to the Landau-Zener mechanism of ballistic electron-hole pair generation. In Sec. III the model of nonequilibrium electron distribution in graphene is presented. The experiment on the excitation of spontaneous optical emission of graphene by high-power THz radiation is described in Sec. IV.[4] In Sec. V,

---

[*]oladyshkin@gmail.com

[1]The situation is different for graphene in a magnetic field (see, e.g., [12]).

[2]The authors of [13] assumed that dislocations could be a possible physical mechanism of such broadening.

---

[3]The currents were obtained from the Schrödinger equation for fermions in graphene [25,26].

[4]The excitation of graphene optical emission by direct current at much smaller fields was studied in [33,34]; optical emission after femtosecond laser excitation was studied in [35].
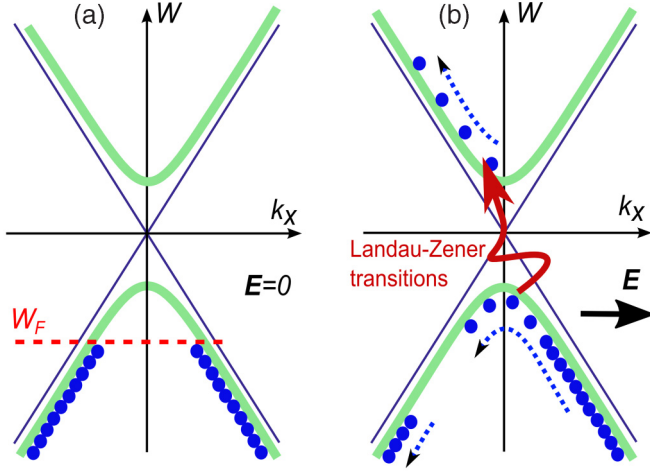
FIG. 1. The interband transition under the action of a THz field. The thick line shows the dependence of the Dirac fermion energy W on quasimomentum k_x for $k_y = $ const. The intersecting thin lines correspond to $k_y = 0$. (a) Initial distribution with the Fermi energy $W_F = $ const. (b) Electron distribution after the modification of initial population near the Dirac point by THz field. The wavy arrow depicts schematically the interband transitions under the action of the THz field.

the dependence of the intensity of the optical emission on the field amplitude of the THz pulse obtained in the experiment is explained within the Landau-Zener theory based on the hypothesis of the decisive role of ballistic interband transitions.

II. THEORETICAL MODEL OF BALLISTIC IONIZATION

The fermion energy spectrum in the neighborhood of the Dirac point has the form [1]

$$W_{c,v} = \pm \hbar v_F \sqrt{k_x^2 + k_y^2},\qquad(1)$$

where $\hbar k_{x,y}$ are the components of the quasimomentum in the single-layer plane and the c and v subscripts define the conducting and valence bands, respectively. Let us consider the $W(k_x)$ dependence at a given value of k_y (Fig. 1).

For $k_y = 0$, the energy diagram is formed by two intersecting straight lines $W_\pm = \pm \hbar v_F k_x$, with the energy sign changing at the point $k_x = 0$ of each line. For $k_y \neq 0$, an energy gap with the width $\Delta W_{\min} = 2\hbar v_F |k_y|$ is formed between the conduction and valence bands.

Let the electric field $\boldsymbol{E} = \boldsymbol{x}_0 E(t)$ be imposed on the system. Changes in the quasimomentum will be described by the classical equations of motion:

$$\hbar \dot{k}_x = -eE, \quad k_y = \text{const}. \qquad(2)$$

If the quantity k_y is regarded as a perturbation defining the splitting of the energy branches (Fig. 1) and $k_x(t)$ is a parameter specifying the difference between the energies of states at each moment of time, then we will obtain a standard Landau-Zener problem [36]. According to the general theory of Landau-Zener transitions, the probability of the interband transition is defined as $P_{\mathrm{LZ}} = \exp(-2\pi\Gamma)$, $\Gamma = \hbar^{-1}(\Delta W_{\min}/2)^2 |\partial(W_+ - W_-)/\partial t|^{-1}$, where the derivative $\partial(W_+ - W_-)/\partial t$ is calculated for the unperturbed (intersect-

ing) branches of the spectrum. In our case, $\partial(W_+ - W_-)/\partial t = 2v_F|eE|$ and the probability of the transition is

$$P_{\mathrm{LZ}} = \exp\left(-\pi \hbar v_F k_y^2 / |eE|\right). \qquad(3)$$

In a general case, within the framework of the Landau-Zener theory the probability of the transition is found by the Wentzel-Kramers-Brillouin (WKB) method as an asymptotic estimate. At the same time, in [28] the probability of transition (3) was found by reducing the Dirac equation to the equation for a parabolic cylinder, for which the WKB estimate coincides with the result of the exact solution. We will assess the characteristic time of the transition and the characteristic size of the region in the momentum space, where the Landau-Zener transitions are significant. It is natural to define the characteristic size of the transition region along the k_y axis by the relation $\delta k_y = \int_{-\infty}^{+\infty} P_{\mathrm{LZ}} dk_y = \sqrt{e\hbar^{-1} v_F^{-1} E}$. The corresponding size of δk_x along the k_x axis will be assessed by doubling the minimal width of the energy gap $\Delta W_{\min}$ corresponding to $k_x^2 \approx 3k_y^2$. Making use of $|k_y| \approx \delta k_y/2$, we obtain $\delta k_x \approx \delta k_y \sqrt{3/2} \approx \sqrt{3eE/2\hbar v_F}$. With allowance for Eq. (2), the time of the quasiparticle flight through the region of electron-hole pair production in the phase space may be estimated to be $\delta t_{\mathrm{LZ}} \approx \hbar \delta k_x/eE \approx \sqrt{\hbar/eEv_F}$.[5] For the $E \approx 100$–$300\,\mathrm{kV/cm}$ fields, this time is $\delta t_{\mathrm{LZ}} \approx 5 - 8\,\mathrm{fs}$. Thus, for a typical THz pulse duration of not less than 100 fs, the transitions may be regarded as almost instantaneous.

Changes in the surface density of conduction electrons $\mathrm{N_c}$ as a result of interband transitions are defined as

$$\dot{N}_c = \int_{-\infty}^{+\infty} P_{\mathrm{LZ}}(\Pi_{x;v} - \Pi_{x;c}) dk_y, \qquad(4)$$

where $\Pi_{x;c,v} = \eta g |\dot{k}_x| n_{c,v}$ are the field-initiated particle fluxes in the k space along the k_x axis in the conduction and valence bands, respectively. In the expressions for $\Pi_{x;c,v}$ fluxes, $n_{c,v}(\boldsymbol{k})$ are the populations that should be specified at the boundary determined above the region of the Landau-Zener transitions. Two terms in the integrand in Eq. (4) correspond to the electron transition from the valence to the conduction band and back;[6] $\eta = 1/4\pi^2$ is the 2D density of the states over the unit area, and $g = 4$ is the degeneracy factor for graphene. By substituting Eqs. (2) and (3) into (4), we obtain

$$\dot{N}_c = \pi^{-2} v_F^{-1/2} |\hbar^{-1} eE|^{3/2} (\langle n_v \rangle - \langle n_c \rangle). \qquad(5)$$

In Eq. (5) the populations $\langle n_{c,v} \rangle$ correspond to the average values for the quasiparticles pulled by the electric field to the boundary of the Landau-Zener transitions in the k space in accordance with the equation of motion (2). For $\langle n_v \rangle = 1$ and $\langle n_c \rangle = 0$ (undoped system), Eq. (5) corresponds to the Schwinger expression for the pair production rate [27,29]. Given that $\langle n_v \rangle = \langle n_c \rangle$, complete compensation of interband

––––––––––––

[5]In the theory of transport processes the quantity $\sqrt{\hbar/v_F eE}$ determines the characteristic threshold time above which the process of Schwinger pair production starts to affect the current-voltage characteristic of a graphene sample [29,32].

[6]Strictly speaking, the $\Pi_{x;c,v}$ fluxes in Eq. (4) should be multiplied by the Pauli blockade factor $(1 - n_{v,c})$; however, all the $n_c n_v$ products decrease in this case.

exchange processes follows from Eq. (5). At the initial moment of time, this regime corresponds to the quasiparticle energies being less than the Fermi energy; it is the reason why the effect of pair production does not influence the current-voltage characteristic of strongly doped graphene [30,31]. At the same time, it follows from Eq. (2) that for the Fermi energy $|W_F| = \hbar v_F k_F$ the region of equal populations is eroded by the field from the neighborhood of the Dirac cone in the momentum space during the time $\delta t_F \approx k_F/|\dot{k}_x| = \hbar k_F/eE$. For the field amplitudes mentioned above and the typical magnitude $|W_F| \approx 0.2$ eV, the time δt_F does not exceed several femtoseconds. This time is much shorter than the indicated characteristic duration of the THz pulse; hence, for such intense fields, we can set in Eq. (5) $\langle n_v \rangle - \langle n_c \rangle \approx 1$, even for relatively heavy initial doping, and obtain

$$N_c \approx \pi^{-2} v_F^{-1/2} |\hbar^{-1} eE|^{3/2} \Delta t_{\text{eff}}, \qquad (6)$$

where Δt_{eff} is the effective duration of a pulse having the amplitude E. The process of the initial population leaving the Dirac point area is schematically shown in Fig. 1.

Let us take, for instance, the data for the THz-induced carrier multiplication reported in [13]. Surface carrier density in the experiments described in [13] was $N_{p0} \approx 6 \times 10^{12}$ cm^{-2} at initial p-type doping and under the action of a THz pulse having a duration $\Delta t_{\text{eff}} \approx 100$ fs increased up to $N_{\text{max1}} \approx 15 \times 10^{12}$ cm^{-2} for the amplitude $E_1 \approx 170$ kV/cm and up to $N_{\text{max2}} \approx 30 \times 10^{12}$ cm^{-2} for $E_2 \approx 300$ kV/cm. Making use of the relationship between the density of the newly born electrons in the conduction band N_c and the total carrier density $N_c = (N_{\text{max}} - N_{p0})/2$ and substituting the values of N_c defined by (6), we will obtain $N_{\text{max1}} \approx 15.4 \times 10^{12}$ cm^{-2} and $N_{\text{max2}} \approx 28 \times 10^{12}$ cm^{-2}. Thus, the estimate (6) gives a fairly good description of the results presented in [13] even when neglecting the decisive role of impact ionization.

III. NONEQUILIBRIUM ELECTRON DISTRIBUTION INDUCED BY THZ PULSE

For applicability of relation (6), the characteristic times δt_{LZ} and δt_{F} found above should be much less than the typical relaxation times. According to [13,14,16–22], typical scattering times of Dirac fermions in graphene τ_{ee} may be tens of femtoseconds, thermalization may range from a hundred to several hundreds of femtoseconds, and cooling may be fractions of picoseconds.[7] The recombination time may exceed the thermalization and cooling times severalfold. Anyhow, even the "fastest" recombination occurs at least not faster than thermalization and cooling (see [20]). These data about the hierarchy of characteristic times of different processes allow us to describe qualitatively the optical emission using a simple model of "bi-Fermi" distribution [30] in the area of the k space where $|k| \gg \delta k_{x,y}$. In this model we set independent chemical potentials for the conduction and valence bands:[8]

$$n_{c,v} = \{\exp[(\pm \hbar v_F k - \mu_{c,v})/T] + 1\}^{-1}. \qquad (7)$$

It is worth noticing that Refs. [22,37] pointed to the possibility of anisotropic relaxation when angular scattering of hot carriers in the conduction band occurs slower than energy thermalization.[9] We will take this into consideration in the optical emission calculation by introducing the anisotropy parameter $\Lambda \leqslant 1$ for the distribution in the region $2v_F k \sim \omega$. This parameter is the ratio of the characteristic angular distribution width to 2π [see the Appendix, Eq. (A21)], and $\Lambda = 1$ corresponds to the isotropic case. Within the framework of the model of bi-Fermi distribution, the spectral photon flux is given by Eq. (A21), which may be represented in the spectral range $\hbar\omega/2 \gg T$, μ_c, $|\mu_v|$ in the form

$$P_\omega = \Lambda P_0(\omega, T) \exp\left(-\frac{\mu_c - \mu_v}{T}\right), \qquad (8)$$

where $P_0(\omega, T) \propto \omega^2 \exp(-\frac{\hbar\omega}{T})$ corresponds to the thermal spectrum in its Wien's part.

Let us find the relationship between the chemical potential μ_c and the surface density N_c of the electrons that have passed to the conduction band from the valence band under the action of a THz pulse. For a degeneracy factor $g = 4$ and density of states $\eta = 1/4\pi^2$ we obtain

$$\int_0^\infty \frac{2x \, dx}{\exp\left(x - \frac{\mu_c}{T}\right) + 1} = \pi \left(\frac{\hbar v_F}{T}\right)^2 N_c. \qquad (9)$$

The chemical potential in the valence band is determined by the surface density of vacancies N_h:

$$\int_0^\infty \frac{2x \, dx}{\exp\left(x + \frac{\mu_v}{T}\right) + 1} = \pi \left(\frac{\hbar v_F}{T}\right)^2 N_h, \qquad (10)$$

where

$$N_h \approx \frac{\mu_v^2(0)}{\pi \hbar^2 v_F^2} + N_c, \qquad (11)$$

And $\mu_v(0) < 0$ is the initial value of the chemical potential for the p-doped degenerate system. Equations (9) and (10) are valid when most of the fermions belong to the isotropic part of the distribution function. Using expression (6) for N_c, we obtain the final equations defining the chemical potentials:

$$-2Li_2\left(-e^{\frac{\mu_c}{T}}\right) = b\varepsilon^{3/2}$$

$$-2Li_2\left(-e^{\frac{\mu_v}{T}}\right) = b\varepsilon^{3/2} + \frac{\mu_v^2(0)}{T^2} \qquad (12)$$

where $Li_2(-e^\zeta) = -\int_0^\infty \frac{x \, dx}{\exp(x - \zeta) + 1}$ is the second-order polylogarithmic function (Fermi-Dirac integral) [38], $b = \frac{\sqrt{\hbar}}{\pi T^2} \Delta t_{\text{eff}} (e v_F E_{\text{THz;max}})^{\frac{3}{2}}$, $\varepsilon = E_{\text{THz}}/E_{\text{THz;max}}$ is the relative magnitude of the field, $E_{\text{THz;max}} = 300$ kV/cm, and $\mu_v(0) < 0$ is the initial value of the chemical potential for a p-doped degenerate system. For the degenerate system and for $\varepsilon \approx 1$, $\Delta t_{\text{eff}} \approx 300$ fs, $\mu_v(0) \approx -0.2$ eV, we obtain $\mu_c \approx 0.6$ eV, $\mu_v \approx -0.7$ eV. In this case, only photons with energies above 1.5 eV correspond to the exponential dependence (8).

---

[7]When $\delta t_F, \delta t_{\text{LZ}} \ll \tau_{ee}$, the following estimation seems to be reasonable: $\langle n_v \rangle - \langle n_c \rangle \approx 1 - \delta t_{\text{LZ}}/\tau_{ee}$.

[8]In this model we suppose a population inversion in the region $\hbar v_F k < |\mu_v|$. However, as shown in [20], such an inversion at times

of the order of cooling time (fractions of picoseconds) is possible even with the most pessimistic assessment of recombination time.

[9]In any case we are concerned with times significantly greater than δt_{LZ} and δt_F.
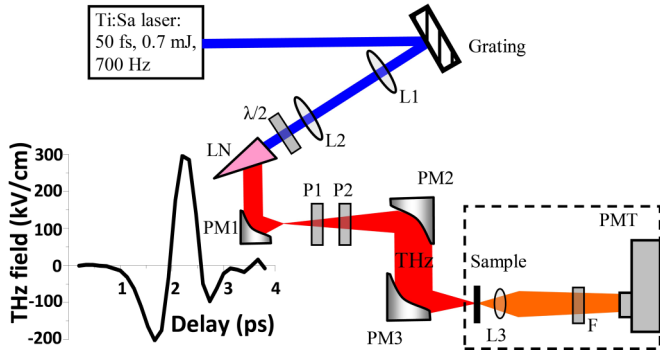
FIG. 2. Experimental setup: L1, L2, L3, lenses; λ/2, λ/2 plate; LN, LiNbO$_3$ crystal; PM1, PM2, PM3, parabolic mirrors; P1, P2, THz polarizers; F, optical filters; PMT, photomultiplier. Inset: time profile of the THz pulse.
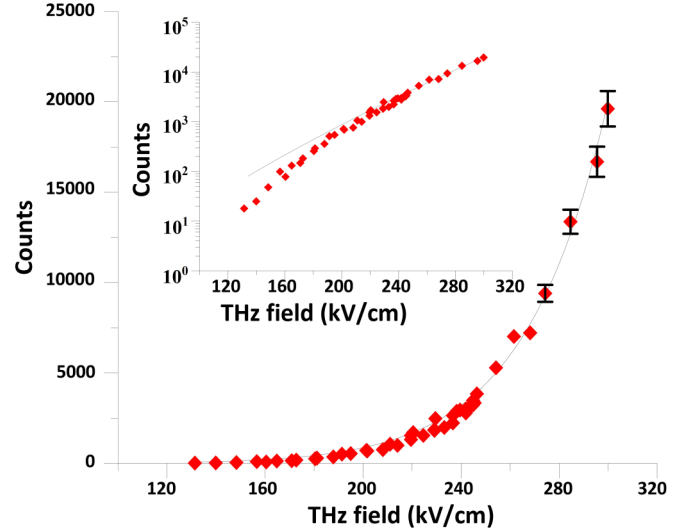

FIG. 3. Number of photons emitted by the graphene sample as a function of the incident terahertz field. The solid line is a fit based on Eqs. (12) and (13) ($E_{THz} = 300\,\text{kV/cm}$ corresponds to the dimensionless variable $\varepsilon = 1$). Inset: the same dependence on a logarithmic scale.

IV. EXPERIMENTAL RESULTS

We measured the number of optical photons (for a wavelength of 340–600 nm) emitted from the graphene sample under the action of a THz pulse. A LiNbO$_3$ crystal irradiated by the Ti:sapphire femtosecond laser (Spitfire, Spectra-Physics) was used as a source of THz radiation. The duration of the optical pulses was 50 fs, its energy was 0.7 mJ, the central wavelength was 795 nm, and the repetition rate was 700 Hz. The technique of a tilted intensity front in a nonlinear LiNbO$_3$ crystal was used to generate THz pulses [39]. The experimental setup is shown in Fig. 2.

The generated THz radiation was collected and transported by means of a telescope consisting of off-axis parabolic mirrors PM1 and PM2 with effective focal lengths (EFLs) of 2.5 and 19 cm, respectively, and was focused on the sample by the parabolic mirror PM3 (EFL = 5 cm). The diameter of the THz spot on the sample was $\approx 500\,\mu\text{m}$ (field amplitude FWHM). The maximum electric field of the THz radiation was 300 kV/cm for a THz pulse energy of 0.4 μJ. The characteristic time profile of THz pulses is presented in the inset in Fig. 2. The THz polarizers P1 and P2 were used for THz attenuation.

In our experiments, we used a monolayer CVD graphene on a borosilicate glass substrate [40]. As the graphene is deposited on glass, substrate-induced inhomogeneity at the graphene-oxide interface gives rise to p-type doping with Fermi energy over 200 meV [13]. Optical emission from the graphene was collected from the solid angle $\Delta o = 0.3\,\text{sr}$ to the photomultiplier (PMT, Hamamatsu R4220P) connected to the photon counting system. A BG39 color filter was placed in front of the PMT to eliminate the leakage 800-nm light. A set of color filters placed before the PMT was used in the experiment when the spectra of optical emission from graphene were investigated.

For the THz field values over 100 kV/cm, optical emission from graphene was detected in the 340–600-nm range. The dependence of the number of graphene-emitted photons accumulated during 6×10^4 laser pulses on the terahertz field magnitude is plotted in Fig. 3. The rise in the optical emission by nearly 3 orders of magnitude was observed with an increase in E_{THz} by a factor of 2. The solid curves in Fig. 3 correspond to the ballistic ionization model (see Sec. III). No

optical emission was observed from the glass substrate without graphene.

The spectrum of optical emission from graphene was retrieved using a set of color filters, taking into consideration the spectral response of our detection system and the spectral characteristics of the color filters. The emission spectra for values of the THz field of 300, 250, and 206 kV/cm are shown in Fig. 4 (it is problematic to reliably retrieve the spectrum for
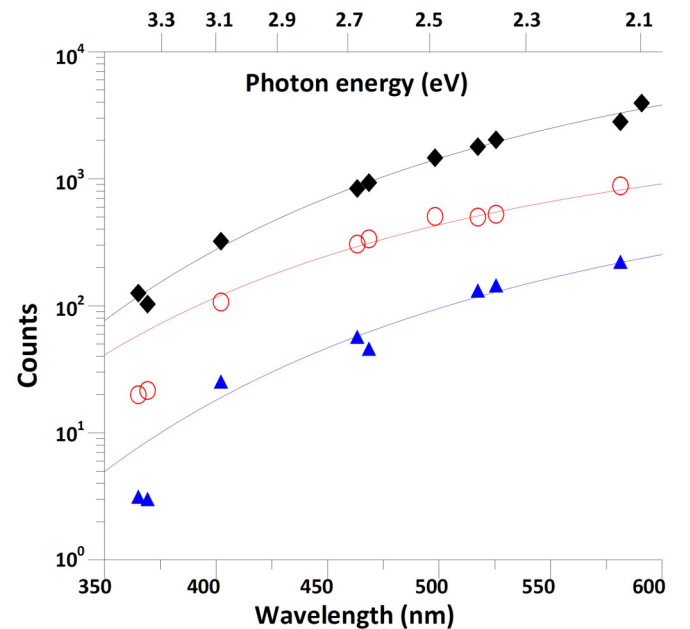

FIG. 4. Measured spectrum of THz-field-excited optical emission. Black rhombs indicate $E_{THz} = 300\,\text{kV/cm}$, $T = 0.25\,\text{eV}$; red circles indicate $E_{THz} = 250\,\text{kV/cm}$, $T = 0.28\,\text{eV}$; and blue triangles indicate $E_{THz} = 206\,\text{kV/cm}$, $T = 0.25\,\text{eV}$. The solid curves correspond to the thermal spectrum in its Wien's part, $\hbar\omega \gg T$.

fields with smaller amplitudes because of the small number of emitted photons).

The lowest photon energy in Fig. 4 corresponds approximately to the value from which exponential dependence (7) should start, as determined in the previous section. The solid curves presented in Fig. 4 were plotted assuming that the spectral photon flux is $P_0(\omega,T) \propto \omega^2 \exp(-\hbar\omega/T)$. The temperature retrieved for the data given in Fig. 4 remains almost unchanged ($T = 0.25 - 0.28$ eV) from the measurement accuracy, while the optical emission increases several tens of times. The effect of saturation of the dependence of the temperature on the field magnitude may be connected to the sharp decrease in the relaxation time of optical phonons with increasing electron energy starting at about 0.2–0.25 eV reported in [35,41].

V. INTERPRETATION OF EXPERIMENTAL DATA AND DISCUSSION

As follows from the data presented in the previous section, with the growth of the THz field amplitude from 200 to 300 kV/cm, the optical emission increases by several tens of times, although the temperature remains unchanged. Such a fast growth of emission intensity despite a nearly constant temperature suggests that not only electron heating but also the electron transition to the conduction band under the action of a THz pulse are significant in this case. Indeed, the spectral intensity of the gray-body radiation depends only on its temperature and the absorption coefficient, in accordance with Kirchhoff's law [for the case of graphene, see the Appendix, Eq. (A19)]. In the discussed range of the photon energies (much greater than the Fermi energy) light absorption in graphene is constant ($\approx 2.3\%$). So the optical radiation observed in our experiments cannot be, in principle, interpreted as a radiation of some equilibrium system.

From Eq. (8), we obtain the total number of detected photons:

$$N_{\det}(\varepsilon) = N_0 \exp\left(\frac{\mu_c - \mu_v}{T}\right). \tag{13}$$

Under the condition of $b\varepsilon^{3/2} \gg 1$, $\mu_v^2(0)/T^2$, Eqs. (12) yield a simple asymptotic dependence $(\mu_c - \mu_v)/T \approx 2\varepsilon^{3/4}\sqrt{2b}$. To calculate the constant N_0 in Eq. (13) we take the expression that follows from Eq. (A21):

$$N_0 = (\pi\alpha)\Upsilon \Lambda \left(\frac{\Delta o}{4\pi}\right)\frac{\Delta t_{\text{em}} A T \Omega^2}{\pi^2 c^2 \hbar},$$

$$\Omega^2 = \int X(\omega)\omega^2 \exp\left(-\frac{\hbar\omega}{T}\right)\frac{\hbar d\omega}{T}. \tag{14}$$

Expressions (14) correspond to the sum of photons of both polarizations emitted into a relatively small solid angle Δo in the direction normal to the single layer of graphene during time Δt_{em} (this time should, evidently, be chosen to be of the order of the cooling time of quasiparticles). Here, $\pi\alpha = \pi e^2/c\hbar \approx 0.023$ is a standard coefficient of interband absorption in graphene, $\Upsilon = 60 \times 10^3$ is the total number of THz shots, and A is the effective area of the emitting single layer. The function $X(\omega)$ is the spectral efficiency of our detection system

accounting for PMT and color filter spectral sensitivity and the influence of the dielectric substrate.[10] Taking $T = 0.2$ eV and numerically calculating Ω^2 in Eqs. (14), we obtain $\Omega^2 \approx 3 \times 10^{24}\,\text{s}^{-2}$. Note that for $N_{\det}(r) \propto \exp\{[\varepsilon(r)]^{3/4}\sqrt{2b}\}$ and the characteristic spatial scale of field localization L_{THz}, the effective area of the emission region is $A \approx L_{\text{THz}}^2/2b$.

Expressions (12) and (13) describe the relative dependence of emission on the THz field amplitude quite well. Only in the region of sufficiently weak fields $E_{\text{THz}}/E_{\text{THz;max}} < 0.5$ does the difference of the theoretical curve from the experimental data, evidently, indicate the appearance of the dependence of the temperature T on the field (in this region the emission is attenuated by about 2 orders of magnitude, as compared to the emission at $E_{\text{THz}} \approx E_{\text{THz;max}}$).

Agreement for absolute values (see Fig. 3) is attained for the parameter values $b = 16$, $\mu_v(0)/T \approx 1$, and $N_0 = 0.4$. These parameters correspond, e.g., to the following reasonable magnitudes: $E_{\text{THz;max}} = 300$ kV/cm, $\Delta o = 0.3$ sr, $\Delta t_{\text{eff}} \approx \Delta t_{\text{em}} \approx 400$ fs, $T = 0.2$ eV, $\Lambda = 0.2$.

In our experiment, the maximal energy of the THz pulse was approximately 0.4 μJ, and the radiated optical energy (in the considered frequency range) corresponded to an efficiency of about 10^{-9}. It is interesting to compare our results with the data from [35], where optical luminescence of graphene irradiated by a 30-fs laser pulse (Ti:sapphire) was studied. The energy efficiency, reported in [35], was also about 10^{-9}, but relative to the absorbed (rather than incident) energy. Since even the unsaturated absorption in a graphene monolayer is lower than 2.3%, our experiment demonstrated much higher efficiency than that in [35]. The probable reason is that THz-induced interband transitions near the Dirac point appeared to be more intense than resonant transitions in the optical field. The characteristic dipole moment in the first case can be estimated as $ev_F \delta t_{\text{LZ}}$, but in the second case it equals the significantly smaller value ev_F/ω.

A more detailed comparison of theory and experiment demands kinetic calculations taking into account a complex form of the THz pulse (see the inset in Fig. 2) and the difference of the fermion distribution from the simple model used above.[11] We intend to carry out such calculations in the near future. Nevertheless, we believe that the conclusion about the determining impact of the Landau-Zener transitions on the process of optical emission excitation is justified already on the basis of the measurements and their interpretation presented in this work.

---

[10]The radiation of the surface current placed on the substrate with dielectric permeability ε_d is attenuated $\sim\varepsilon_d^{-1}$ times. Also the optical radiation is refracted at the other substrate surface, which gives again the $\sim\varepsilon_d^{-1}$ factor due to the angular spectrum spreading.

[11]These calculations may provide a more accurate definition of Δt_{eff} and elucidate its dependence on relative field amplitude ε.

APPENDIX: SPONTANEOUS EMISSION OF A GRAPHENE MONOLAYER

1. Basic equations

Consider massless Dirac fermions in the emission field using the Hamiltonian of the system

$$
\hat{H} = \sum_{\nu,q} \hbar\omega_q \left(\hat{c}_{\nu q}^\dagger \hat{c}_{\nu q} + \frac{1}{2} \right) + \sum_{sk} W_s(k)\hat{a}_{sk}^\dagger \hat{a}_{sk}
$$
$$
+ \sum_{ss'kk'} \hat{V}_{ss'kk'}\hat{a}_{sk}^\dagger \hat{a}_{s'k'}. \tag{A1}
$$

Here, $\hat{c}_{\nu q}^\dagger$ and $\hat{c}_{\nu q}$ are the operators of creation and annihilation of Fock photon states $|n_{\nu q}\rangle$ corresponding to wave vector q, the subscript ν stands for photon polarization, and $\omega_q^2 = c^2 q^2$. The fermions are described by the creation and annihilation operators $\hat{a}_{sk}^\dagger$ and $\hat{a}_{sk}$ corresponding to massless Dirac states $|k,s\rangle$ [42]:

$$
|k,s\rangle = \frac{e^{ikr}}{\sqrt{2A}} \begin{pmatrix} s \\ e^{i\theta(k)} \end{pmatrix}, \quad W_s(k) = s\hbar\upsilon_F k, \tag{A2}
$$

where A is the area of a monolayer lying in the xy plane, k is the 2D wave vector of a quasiparticle, the indices $s = \pm 1$ correspond to the eigenfunctions for the conduction and valence bands, respectively, and $\theta(k)$ is the angle between the quasimomentum and the x axis. Summation over k in Eq. (A1) formally implies summation over spin states and valleys.

In Eq. (A1) $\hat{V}_{ss'kk'}$ is the matrix element of the interaction operator [42], which in the case of a quantum field must depend on the $\hat{c}_{\nu q}^\dagger$ and $\hat{c}_{\nu q}$ operators:

$$
\hat{V} = -\frac{1}{c}\hat{j}\hat{A}, \tag{A3}
$$

where $\hat{j} = -e\upsilon_F \hat{\sigma}$ is the operator of the current, $\hat{\sigma} = x_0\hat{\sigma}_x + y_0\hat{\sigma}_y$, $\hat{\sigma}_x$ and $\hat{\sigma}_y$ are the Pauli matrices, $\hat{A}$ is the vector potential operator

$$
\hat{A} = \sum_{\nu,q} \sqrt{\frac{2\pi c^2\hbar}{V\omega_q}} \cdot (e_\nu \hat{c}_{\nu q} e^{-i\omega_q t + iqr} + e_\nu^* \hat{c}_{\nu q}^\dagger e^{i\omega_q t - iqr}), \tag{A4}
$$

and V is quantization volume. Let $\nu = S, P$ correspond to standard S and P polarizations of photons; that is, the unit vector e_S lies in the monolayer plane, and the unit vector e_P lies in the plane formed by vector q and the normal to the monolayer. The direction of vector q is specified by the angle Θ_q relative to the normal of the monolayer and by the angle Φ_q relative to the x axis in the xy plane. For such polarization vectors, the case $\Theta_q = 0$ is degenerate: we can consider for this case photons polarized along the x and y axes; that is, we can take $\nu = x, y$.

Expressions for the matrix elements $\hat{V}_{ss'kk'}$ are obtained taking into consideration the reasonable condition $q \ll k$. For this approximation we will have

$$
\hat{V}_{+1+1kk'} \approx e\upsilon_F \sum_q \sqrt{\frac{2\pi\hbar}{V\omega_q}} [\sin(\Phi_q - \theta)(\delta_{k(k'+q_\perp)}\hat{c}_{Sq}e^{-i\omega_q t} + \delta_{k(k'-q_\perp)}\hat{c}_{Sq}^\dagger e^{i\omega_q t})
$$
$$
+ \cos\Theta_q\cos(\Phi_q - \theta)(\delta_{k(k'+q_\perp)}\hat{c}_{Pq}e^{-i\omega_q t} + \delta_{k(k'-q_\perp)}\hat{c}_{Pq}^\dagger e^{i\omega_q t})], \tag{A5}
$$

$$
\hat{V}_{+1-1kk'} \approx ie\upsilon_F \sum_q \sqrt{\frac{2\pi\hbar}{V\omega_q}} [\cos(\Phi_q - \theta)(\delta_{k(k'+q_\perp)}\hat{c}_{Sq}e^{-i\omega_q t} + \delta_{k(k'-q_\perp)}\hat{c}_{Sq}^\dagger e^{i\omega_q t})
$$
$$
- \cos\Theta_q\sin(\Phi_q - \theta)(\delta_{k(k'+q_\perp)}\hat{c}_{Pq}e^{-i\omega_q t} + \delta_{k(k'-q_\perp)}\hat{c}_{Pq}^\dagger e^{i\omega_q t})], \tag{A6}
$$

$$
\hat{V}_{-1-1kk'} = -\hat{V}_{+1+1kk'}, \quad \hat{V}_{-1+1kk'} = -\hat{V}_{+1-1kk'}, \tag{A7}
$$

where $q_\perp$ is the vector component q in the plane of the graphene monolayer: $q_\perp = q|\sin\Theta_q|$.

2. Probability of interband spontaneous transition

Consider a spontaneous transition between the states $|k', +1\rangle \rightarrow |k, -1\rangle$ accompanied by photon emission with ν-type polarization. For the probability of such a transition per unit time w_ν we can right away use Fermi's golden rule [43]:

$$
w_\nu = \frac{2\pi}{\hbar} \int d\Pi_f |V_{\nu,\text{fi}}|^2 \delta(W_i - W_f - \hbar\omega). \tag{A8}
$$

The integration $\int d\Pi_f$ in (A8) is done over all final states of the system, i is the initial state, and $\hbar\omega$ is the photon energy. In this case we have $W_i = \hbar\upsilon_F k', W_f = -\hbar\upsilon_F k$; the matrix element $V_{\nu,\text{fi}}$ is $V_{\nu,\text{fi}} = \langle 1_{\nu q}|\hat{V}_{-1+1kk'}|0_{\nu q}\rangle$, where $|n_{\nu q}\rangle$ is the corresponding Fock state, and we obtain

$$
|V_{S,\text{fi}}|^2 = e^2\upsilon_F^2\cos^2[\Phi_q - \theta(k)]\frac{2\pi\hbar}{V\omega_q}\delta_{k(k'-q_\perp)}, \tag{A9a}
$$

$$
|V_{P,\text{fi}}|^2 = e^2\upsilon_F^2\cos^2\Theta_q\sin^2[\Phi_q - \theta(k)]\frac{2\pi\hbar}{V\omega_q}\delta_{k(k'-q_\perp)}. \tag{A9b}
$$

The emitted photon frequency is determined by the condition $W_i - W_f = \hbar\omega$. Taking into consideration the relations $\omega = 2\upsilon_F(|\boldsymbol{k}| + |\boldsymbol{k} + \boldsymbol{q}_\perp|)$ and $q = c/\omega$ and the inequality $q \ll k$, we obtain

$$\omega \approx \frac{2\upsilon_F k}{1 + \frac{\upsilon_F}{c}\sin\Theta_q\cos[\Phi_q - \theta(\boldsymbol{k})]}. \qquad (A10)$$

Further, with the expression for the density of states of photons with given polarization in Eq. (A8) taken into account, we have $d\Pi_f = (2\pi c)^{-3}V\omega^2 d\omega d\Omega$, where $d\Omega = \sin\Theta_q d\Theta_q d\Phi_q$ is the element of the solid angle in the direction of the photon wave vector $\boldsymbol{q}$. The substitution of Eqs. (A9a) and (A9b) into Eq. (A8) yields the expression for the probability of spontaneous emission into a unit solid angle:

$$w_{\Omega;S} = \frac{e^2\upsilon_F^2\omega}{2\pi\hbar c^3}\cos^2[\Phi_q - \theta(\boldsymbol{k})], \qquad (A11a)$$

$$w_{\Omega;P} = \frac{e^2\upsilon_F^2\omega}{2\pi\hbar c^3}\cos^2\Theta_q\sin^2[\Phi_q - \theta(\boldsymbol{k})], \qquad (A11b)$$

where the emitted photon frequency is specified by relation (A10).

3. Summation over electron states

Let us sum expressions (A11a) and (A11b) over 2D electron states:

$$\sum_{\boldsymbol{k}}(\cdots) \Rightarrow \frac{gA}{4\pi^2}\int_\infty(\cdots)d^2k = \frac{gA}{4\pi^2}$$
$$\times \int_0^{2\pi}d\theta\int_0^\infty(\cdots)kdk, \qquad (A12)$$

where $g = 4$ is the factor of degeneracy with respect to spin states and valleys. Making use of the approximate relation $\omega = 2\upsilon_F k$ following from Eq. (A10), via Eqs. (A11a) and (A11b) and Eq. (A12), we obtain an expression for spectral photon fluxes $P_{\omega\Omega;S,P}$:

$$\begin{bmatrix} P_{\omega\Omega;S} \\ P_{\omega\Omega;P} \end{bmatrix} = \frac{A\omega^2}{2^3\pi^4c^2}(\pi\alpha)\int_0^{2\pi}\begin{bmatrix} \cos^2(\Phi_q - \theta) \\ \cos^2\theta_q\sin^2(\Phi_q - \theta) \end{bmatrix}$$
$$\times \{n_c(k,\theta)[1 - n_\upsilon(k,\theta)]\}_{k=\omega/2\upsilon_F}d\theta, \qquad (A13)$$

where $\pi\alpha = \pi e^2/c\hbar \approx 0.023$ is a standard coefficient of interband absorption in graphene, $n_{c,\upsilon}(k,\theta) = \langle\hat{a}_{\pm1\boldsymbol{k}}^\dagger\hat{a}_{\pm1\boldsymbol{k}}\rangle$ are average occupation numbers of photon states (populations), and $1 - n_\upsilon$ is the Pauli blockade factor. For fermion distributions isotropic with respect to angle θ, from Eq. (A13) it follows that

$$\begin{bmatrix} P_{\omega\Omega;S} \\ P_{\omega\Omega;P} \end{bmatrix} = \frac{A\omega^2}{(2\pi)^3c^2}\begin{bmatrix} 1 \\ \cos^2\theta_q \end{bmatrix}\pi\alpha\{n_c(k)[1 - n_\upsilon(k)]\}_{k=\omega/2\upsilon_F}. \qquad (A14)$$

4. Emission of the equilibrium ensemble of quasiparticles

Consider the Fermi distribution

$$n_{c,\upsilon} = \left[\exp\left(\frac{\pm\hbar k\upsilon_F + \mu}{T}\right) + 1\right]^{-1}. \qquad (A15)$$

The substitution of (A15) into (A14) yields

$$\begin{bmatrix} P_{\omega\Omega;S}(T) \\ P_{\omega\Omega;P}(T) \end{bmatrix} = \begin{bmatrix} 1 \\ \cos^2\Theta_q \end{bmatrix}\frac{A\omega^2}{(2\pi)^3c^2}$$
$$\times \frac{\pi\alpha}{\left[\exp\left(\frac{\hbar\omega/2+\mu}{T}\right) + 1\right]\left[\exp\left(\frac{\hbar\omega/2-\mu}{T}\right) + 1\right]}. \qquad (A16)$$

To confirm the correctness of calculating luminescence we will show that Eq. (A16) corresponds to the Kirchhoff law. Indeed, following [42], we can readily obtain an expression for monolayer optical thickness determined by interband absorption for isotropic distributions $n_{c,\upsilon}(k)$ at an arbitrary value of Θ_q:

$$\begin{bmatrix} \Gamma_S \\ \Gamma_P \end{bmatrix} = \begin{bmatrix} \cos^{-1}\theta_q \\ \cos\theta_q \end{bmatrix}\pi\alpha[n_\upsilon(k) - n_c(k)]_{k=\omega/2\upsilon_F} \qquad (A17)$$

(for $\theta_q \ll 1$ and $n_c = 0$, $n_\upsilon = 1$ we obtain $\Gamma_{S,P} = \pi\alpha$). For the equilibrium distribution (A15), from Eq. (A17) it follows that

$$\begin{bmatrix} \Gamma_S(\omega,T) \\ \Gamma_P(\omega,T) \end{bmatrix} = \begin{bmatrix} \cos^{-1}\Theta_q \\ \cos\Theta_q \end{bmatrix}\pi\alpha$$
$$\times \frac{\left[\exp\left(\frac{\hbar\omega}{T}\right) - 1\right]}{\left[\exp\left(\frac{\hbar\omega/2+\mu}{T}\right) + 1\right]\left[\exp\left(\frac{\hbar\omega/2-\mu}{T}\right) + 1\right]}. \qquad (A18)$$

A comparison of Eqs. (A16) and (A18) gives

$$P_{\omega\Omega;S,P}(T) = \Gamma_{S,P}(\omega,T)A\cos\Theta_q P_0(\omega,T), \qquad (A19)$$

where $P_0(\omega,T) = \frac{\omega^2}{(2\pi)^3c^2}[\exp(\frac{\hbar\omega}{T}) - 1]^{-1}$ is the spectral flux of photons with fixed polarization through unit area in unit solid angle [43]. The expression (A19) explicitly expresses Kirchhoff's law.

5. Spontaneous emission of bi-Fermi distribution

Let there occur in each band a distribution with its own chemical potential

$$n_{c,\upsilon} = \left[\exp\left(\frac{\pm\hbar k\upsilon_F - \mu_{c,\upsilon}}{T}\right) + 1\right]^{-1}. \qquad (A20)$$

We will find the spectral photon flux into the lens placed above the emitting area at an angle $\Theta_q = 0$ collecting photons of both polarizations from a relatively small solid angle Δo. We consider Wien's region of the spectrum ($\hbar\omega/2 \mp \mu_{c,\upsilon} \gg T$) and use expressions (A13) and (A20). We will qualitatively allow for possible anisotropy of high-energy ($2\upsilon_F k \sim \omega$) carrier distribution assuming $n_c \neq 0$ in the sector $-\Delta\theta/2 < \theta < \Delta\theta/2$ to obtain

$$P_\omega \approx \left(\frac{\Delta o}{4\pi}\right)\frac{\Lambda A\omega^2}{\pi^2 c^2}\pi\alpha\exp\left(-\frac{\hbar\omega}{T}\right)\exp\left(\frac{\mu_c - \mu_\upsilon}{T}\right), \qquad (A21)$$

where $\Lambda \leqslant 1$ is the anisotropy parameter. Within the framework of the considered simple model $\Lambda = \Delta\theta/2\pi$.

Instead of the above simplest model of anisotropic angular distribution, a standard method of Legendre polynomial expansion may be used. Taking into account the first two terms of the Legendre series, under the condition $n_c \leqslant 1$, we obtain the expression

$$n_c = \left[\exp\left(\frac{\hbar k v_F - \mu_c}{T} \right) + 1 \right]^{-1} [1 - \lambda(1 - \cos\theta)]. \tag{A22}$$

It can be readily ascertained that the use of Eq. (A22) also leads to Eq. (A21), where $1 - \lambda = \Lambda$.

---

[1] F. Bonaccorso, Z. Sun, T. Hasan, and A. C. Ferrari, Nat. Photon. **4**, 611 (2010).

[2] N. Kumar, J. Kumar, C. Gerstenkorn, R. Wang, H.-Y. Chiu, A. L. Smirl, and H. Zhao, Phys. Rev. B **87**, 121406 (2013).

[3] M. Tokman, X. Yao, and A. Belyanin, Phys. Rev. Lett. **110**, 077404 (2013).

[4] J. L. Cheng, N. Vermeulen, and J. E. Sipe, Opt. Express **22**, 15868 (2014).

[5] H. K. Avetissian, A. K. Avetissian, G. F. Mkrtchian, and K. V. Sedrakian, J. Nanophotonics **6**, 061702 (2012).

[6] M. M. Glazov and S. D. Ganichev, Phys. Rep. **535**, 101 (2014).

[7] E. Hendry, P. J. Hale, J. Moger, A. K. Savchenko, and S. A. Mikhailov, Phys. Rev. Lett. **105**, 097401 (2010).

[8] S. A. Mikhailov, Phys. Rev. B **90**, 241301(R) (2014).

[9] X. Yao, M. Tokman, and A. Belyanin, Phys. Rev. Lett. **112**, 055501 (2014).

[10] T. J. Constant, S. M. Hornett, D. E. Chang, and E. Hendry, Nat. Phys. **12**, 124 (2015).

[11] T. Otsuji, S. A. Boubanga Tombet, A. Satou, H. Fukidome, M. Suemitsu, E. Sano, V. Popov, M. Ryzhii, and V. Ryzhii, J. Phys. D **45**, 303001 (2012).

[12] Y. Wang, M. Tokman, and A. Belyanin, Phys. Rev. A **91**, 033821 (2015).

[13] S. Tani, F. Blanchard, and K. Tanaka, Phys. Rev. Lett. **109**, 166603 (2012).

[14] K. J. Tielrooij, J. C. W. Song, S. A. Jensen, A. Centeno, A. Pesquera, A. Zurutuza Elorza, M. Bonn, L. S. Levitov, and F. H. L. Koppens, Nat. Phys. **9**, 248 (2013).

[15] M. S. Foster and I. L. Aleiner, Phys. Rev. B **79**, 085415 (2009).

[16] M. Mittendorff, T. Winzer, E. Malic, A. Knorr, C. Berger, W. A. de Heer, H. Schneider, M. Helm, and S. Winnerl, Nano Lett. **14**, 1504 (2014).

[17] D. Brida, A. Tomadin, C. Manzoni, Y. J. Kim, A. Lombardo, S. Milana, R. R. Nair, K. S. Novoselov, A. C. Ferrari, G. Cerullo, and M. Polini, Nat. Commun. **4**, 1987 (2013).

[18] T. Ploetzing, T. Winzer, E. Malic, D. Neumaier, A. Knorr, and H. Kurz, Nano Lett. **14**, 5371 (2014).

[19] T. Winzer, E. Malic, and A. Knorr, Phys. Rev. B **87**, 165413 (2013).

[20] T. Winzer, A. Knorr, and E. Malic, Nano Lett. **10**, 4839 (2010).

[21] E. Malic, T. Winzer, E. Bobkin, and A. Knorr, Phys. Rev. B **84**, 205406 (2011).

[22] E. Malic, T. Winzer, and A. Knorr, Appl. Phys. Lett. **101**, 213110 (2012).

[23] P. Bowlan, E. Martinez-Moreno, K. Reimann, M. Woerner, and T. Elsaesser, New J. Phys. **16**, 013027 (2014).

[24] P. Bowlan, E. Martinez-Moreno, K. Reimann, T. Elsaesser, and M. Woerner, Phys. Rev. B **89**, 041408(R) (2014).

[25] K. L. Ishikawa, Phys. Rev. B **82**, 201402(R) (2010).

[26] K. L. Ishikawa, New J. Phys. **15**, 055021 (2013).

[27] O. Vafek and A. Vishwanath, Annu. Rev. Condens. Matter Phys. **5**, 83 (2014).

[28] N. Yokomizo, Ann. Phys. (NY) **351**, 166 (2014).

[29] S. Vajna, B. Dora, and R. Moessner, Phys. Rev. B. **92**, 085122 (2015).

[30] G. Kane, M. Lazzeriand, and F. Mauri, J. Phys. Condens. Matter. **27**, 164205 (2015).

[31] N. Vandecasteele, A. Barreiro, M. Lazzeri, A. Bachtold, and F. Mauri, Phys. Rev. B **82**, 045416 (2010).

[32] M. Lewkowicz, B. Rosenstein, and D. Nghiem, Phys. Rev. B **84**, 115419 (2011).

[33] S. Berciaud, M. Y. Han, K. F. Mak, L. E. Brus, P. Kim, and T. F. Heinz, Phys. Rev. Lett. **104**, 227401 (2010).

[34] M. Freitag, H.-Y. Chiu, M. Steiner, V. Perebeinos, and P. Avouris, Nat. Nanotechnol. **5**, 497 (2010).

[35] C. H. Lui, K. F. Mak, J. Shan, and T. F. Heinz, Phys. Rev. Lett. **105**, 127404 (2010).

[36] C. Cohen-Tannoudji, B. Diu, and F. Laloe, *Quantum Mechanics* (Wiley, New York, 1977), Vol. 1.

[37] J. C. König-Otto, M. Mittendorff, T. Winzer, F. Kadi, E. Malic, A. Knorr, C. Berger, W. A. de Heer, A. Pashkin, H. Schneider, M. Helm, and S. Winnerl, Phys. Rev. Lett. **117**, 087401 (2016).

[38] I. S. Gradshteyn and I. M. Ryzhik, in *Table of Integrals, Series, and Products*, edited by D. Zwillinger and V. Moll, 8th ed. (Elsevier, 2014).

[39] J. A. Fulop, L. Palfalvi, G. Almasi, and J. Hebling, Opt. Express **18**, 12311 (2010).

[40] See https://graphene-supermarket.com

[41] H. Wang, J. H. Strait, P. A. George, S. Shivaraman, V. B. Shields, M. Chandrashekhar, J. Hwang, F. Rana, M. G. Spencer, C. S. Ruiz-Vargas, and J. Park, Appl. Phys. Lett. **96**, 081917 (2010).

[42] M. I. Katsnelson, *Graphene: Carbon in Two Dimensions* (Cambridge University Press, New York, 2012).

[43] V. B. Berestetskii, E. M. Lifshitz, and L. P. Pitaevskii, *Quantum Electrodynamics* (Butterworth-Heinemann, Oxford, 1982).